Chemistry–A European Journal
Research Article
doi.org/10.1002/chem.202200510
Chemistry Europe
European Chemical Societies Publishing
www.chemeurj.org

Red Light-Emitting Thermally-Activated Delayed Fluorescence of Naphthalimide-Phenoxazine Electron Donor-Acceptor Dyad: Time-Resolved Optical and Magnetic Spectroscopic Studies

Xue Zhang[+,a] Xiao Liu[+,a] Maria Taddei[+,b] Laura Bussotti,[b] Ivan Kurganskii,[c] Minjie Li,[d] Xiao Jiang,[e] Longjiang Xing,[f] Shaomin Ji,[f] Yanping Huo,[f] Jianzhang Zhao,*[a] Mariangela Di Donato,*[b, g] Yan Wan,*[d] Zujin Zhao,*[h] and Matvey V. Fedin*[c]

Abstract: We prepared an orthogonal compact electron-donor (phenoxazine, PXZ)-acceptor (naphthalimide, NI) dyad (**NI-PXZ**), to study the photophysics of the thermally-activated delayed fluorescence (TADF), which has a luminescence lifetime of 16.4 ns (99.2 %)/17.0 μs (0.80 %). A weak charge transfer (CT) absorption band was observed for the dyad, indicating non-negligible electronic coupling between the donor and acceptor at the ground state. Femtosecond transient absorption spectroscopy shows a fast charge separation (CS) (ca. 2.02 ~ 2.72 ps), the majority of the singlet CS state is short-lived, especially in polar solvents (τ_{CR} = 10.3 ps in acetonitrile, vs. 1.83 ns in toluene, 7.81 ns in *n*-hexane). Nanosecond transient absorption spectroscopy detects a long-lived transient species in *n*-hexane, which is with a mixed triplet local excited state (^{3}LE) and charge separated state (^{3}CS), the lifetime is 15.4 μs. In polar solvents, such as tetrahydrofuran and acetonitrile, a neat ^{3}CS state was observed, whose lifetimes are 226 ns and 142 ns, respectively. Time-resolved electron paramagnetic resonance (TREPR) spectra indicate the existence of strongly spin exchanged ^{3}LE/^{3}CT states, with the effective zero field splitting (ZFS) $|D|$ and $|E|$ parameters of 1484 MHz and 109 MHz, respectively, much smaller than that of the native ^{3}NI state (2475 and 135 MHz). It is rare but solid experimental evidence that a closely-lying ^{3}LE state is crucial for occurrence of TADF and this ^{3}LE state is an essential intermediate state to facilitate reverse intersystem crossing in TADF systems.

Introduction

Triplet photosensitizers (PSs) are compounds showing strong light absorption, efficient intersystem crossing (ISC), appropriate redox potentials and good photo- and chemo-stability.[1] Triplet PSs have been widely used in photodynamic therapy (PDT),[1b,c,2] phosphorescent O_2 sensing,[3] photocatalysis,[1a,4] photon upconversion, etc.[5] ISC is one of the most critical parameters for triplet PSs,[6] an electron spin forbidden process. Magnetic torque is required to facilitate the electron spin rephasing or flip during ISC. One of the most popular methods to enhance ISC in organic chromophores is exploiting the spin orbit

[a] *X. Zhang,[+] X. Liu,[+] Prof. J. Zhao*
State Key Laboratory of Fine Chemicals
School of Chemical Engineering
Dalian University of Technology
Dalian 116024 (P. R. China)
E-mail: zhaojzh@dlut.edu.cn

[b] *Dr. M. Taddei,[+] L. Bussotti, Prof. M. Di Donato*
LENS (European Laboratory for Non-Linear Spectroscopy)
via N. Carrara 1, 50019 Sesto Fiorentino (FI) (Italy)
E-mail: didonato@lens.unifi.it

[c] *I. Kurganskii, Prof. M. V. Fedin*
International Tomography Center, SB RAS, and
Novosibirsk State University
630090 Novosibirsk (Russia)
E-mail: mfedin@tomo.nsc.ru

[d] *M. Li, Prof. Y. Wan*
College of Chemistry
Beijing Normal University
Beijing 100875 (P. R. China)
E-mail: wanyan@bnu.edu.cn

[e] *Dr. X. Jiang*
Key Laboratory of Industrial Ecology and Environmental Engineering (MOE)
School of Environmental Science and Technology
Dalian University of Technology
Dalian 116024 (P. R. China)

[f] *L. Xing, Prof. S. Ji, Prof. Y. Huo*
Light Industry and Chemical Engineering College
Guangdong University of Technology
Guangzhou 510006, (P. R. China)

[g] *Prof. M. Di Donato*
ICCOM-CNR
via Madonna del Piano 10–12, 50019 Sesto Fiorentino (FI) (Italy)

[h] *Prof. Z. Zhao*
State Key Laboratory of Luminescent Materials and Devices
South China University of Technology
Guangzhou 510640 (P. R. China)
E-mail: mszjzhao@scut.edu.cn

[+] *These authors contributed equally to this work.*

Supporting information for this article is available on the WWW under https://doi.org/10.1002/chem.202200510

coupling (SOC) effect, with the attaching of heavy atoms, such as Pt, Ir, Ru, I or Br, to the chromophore.[6a] Another method is to attain two states (singlet and triplet) with similar energy, respectively presenting n–π* and π–π* character, as to satisfy the El Sayed's rule and enhance ISC.[7] Other approaches have also been used to enhance ISC, for instance, exciton coupling,[8] or the use an electron spin converter such as C_{60},[9] the recourse to radical enhanced ISC,[10] or the induction of ISC through a twisted π-conjugation system.[11] These methods are based on different molecular structural profiles, and have produced triplet PSs that have been used in PDT, photo-redox catalytic organic reactions, photon upconversion, etc. However, these methods suffer from some disadvantages, for example high cost of preparation, difficult synthesis, or shortened triplet state lifetimes. Therefore, new methods to enhance ISC and to solve the above mentioned challenges are highly desired.

Concerning this aspect, charge recombination (CR)-induced ISC is of particular interest.[12] The traditional electron donor-acceptor dyads showing CR-induced ISC have been mainly developed to mimic the natural photosynthetic reaction center, and to attain long-lived charge separated (CS) states, with the electron donor and acceptor separated by large distances.[12a,13] In this case, the electronic coupling and the CR rate constant are reduced, which makes the charge transfer (CT) state long lived. Most often these dyads are difficult to synthesize, because they require long and rigid linkers. In *compact* electron donor-acceptor dyads, i.e. dyads with a short linker between the donor and acceptor, however, the electronic coupling is large, which inhibits both the $^1CS\rightarrow {}^3CS$ ISC (radical pair ISC, RP-ISC, enhanced by hyperfine coupling interactions), and the generation of low-lying ^3LE states (LE: locally excited) via $^3CS\rightarrow {}^3LE$.[12a] Interestingly, it was found recently that in the *compact* dyads, ISC is favored given the electron donor and acceptor adopt a mutual *orthogonal* orientation (perpendicular geometry): in this case, the so-called spin orbit charge transfer ISC (SOCT-ISC) occurs. According to this mechanism, the CR process is accompanied with a change of molecular orbital angular momentum, which off-sets the change of electron spin angular momentum associated with the ISC, thus enhancing ISC.[14] Although some dyads showing SOCT-ISC have been reported, it is clear that much room is left for further studies in this field. Previous investigations indicate that the electron spin polarization (ESP) phase pattern of the triplet state time-resolved electron paramagnetic resonance (TREPR) spectrum, i.e. the electron spin selectivity of the ISC, is dependent on the mutual orientation of the donor and acceptor.[14b] However, one of our recent studies showed that the structure of the electron donor (or acceptor) also contribute to the ESP.[15] Moreover, although it was previously assumed that the ESP is ISC-specific, our recent results show this may be not always the case.[14c]

If the ^3LE state of the electron donor or acceptor chromophore is energetically close to the CS state, thermally activated delayed fluorescence (TADF) may be observed.[16] In almost decoupled dyads, the electron exchange energy in frontier orbitals of the radical pair is small, i.e. $2J$, usually $<0.1\ cm^{-1}$, thus the energy gap between ^1CS and ^3CS states is small. This implies that TADF can be considered as a special case in the orthogonal *compact* dyads showing SOCT-ISC, with the ^3LE state share similar energy with the CS state.[17] Only a few examples of molecules showing TADF and SOCT-ISC have been reported, so that an in-depth analysis of the electronic configuration of the excited states of these systems is necessary.[16a,18]

In order to address the above challenges, we prepared a compact orthogonal dyad, with naphthalimide (NI) as electron acceptor and phenoxazine (PXZ) as electron donor (**NI-PXZ**. Scheme 1). The photophysical properties of the dyad were studied with steady state and time-resolved UV/Vis absorption and luminescence spectroscopic methods, and TADF was observed for the dyad. The CS and CR rate constants were determined with femtosecond and nanosecond transient absorption spectroscopy. With the support of TREPR spectroscopy, we show that the transient species formed in **NI-PXZ** upon photoexcitation has a mixed ^3LE and ^3CS character, and it is not a fully charge separated state. This information is useful for an in-depth understanding of the excited state processes in electron donor-acceptor dyads, and for clarifying the electronic configuration of the excited states of TADF molecules.

Results and Discussion

Design and synthesis of the compounds

NI is a popular chromophore in photochemistry and photophysics,[19] and presents a triplet state with high energy ($E_T = 2.29$ eV).[20] By connecting it with the PXZ unit, which is an electron donor,[21] the electron donor-acceptor dyad **NI-PXZ** is prepared (Scheme 1). Due to the steric hindrance of the *peri*-H atoms on the PXZ and on the NI moieties, we expect an orthogonal geometry for the dyad. We reported an analogue

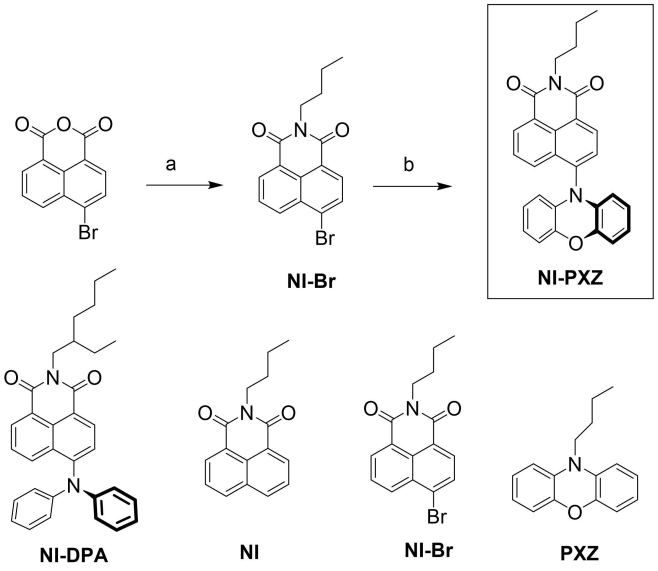

Scheme 1. Synthesis procedures of the compounds. a) *n*-Butylamine, ethanol, reflux, 80 °C, 10 h, yield: 32%; b) Phenoxazine, $Pd(OAc)_2$, $P(t\text{-}Bu)_3HBF_4$, *t*-BuONa, toluene, reflux, 8 h, yield: 54%.

NI-phenothiazine (PTZ) dyad recently,[16a] and we have shown that one-atom substitution may induced different photophysical properties,[22] with the ESP not only dependent on the geometry, but also on the structure of the electron donor or acceptor.[15] Therefore, it is worth to study **NI-PXZ** compound. The oxidation potential of the PXZ (E_{OX} = ca. +0.22 V vs. Fc/Fc^+) is slightly smaller compared to PTZ (E_{OX} = ca. +0.30 V vs. Fc/Fc^+),[23] thus we expect different properties for **NI-PXZ** and **NI-PTZ**, due to a variation of the CS state energy, and its matching with the ^{3}LE state.[16a] During the preparation of this manuscript, applications of dyads analogue to **NI-PXZ** in organic light-emitting diodes (OLED) or bioimaging were reported, but a detailed photophysical study was not presented.[24]

Buchwald-Hartwig coupling reaction was used for the preparation of the **NI-PXZ** dyad with C–N connection (Scheme 1).[16a] In order to attain an in-depth understanding of the photophysical properties of the dyad, we used **NI**, **NI-Br** and **NI-DPA** as reference compounds (Scheme 1).

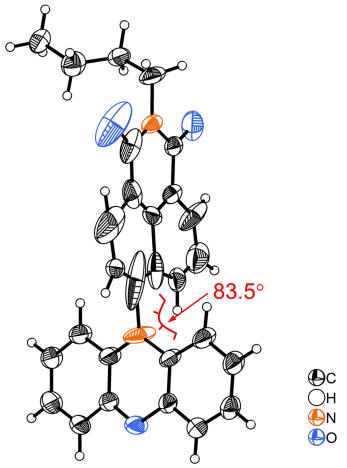

Figure 1. ORTEP view of the molecular structure of **NI-PXZ** determined with single crystal X-ray diffraction. The dihedral angle (83.5°) between the phenothiazine and naphthalimide moiety is indicated. Thermal ellipsoids are at 50% probability. Deposition Number 2150272 (for **NI-PXZ**) contains the supplementary crystallographic data for this paper. These data are provided free of charge by the joint Cambridge Crystallographic Data Centre and Fachinformationszentrum Karlsruhe Access Structures service.

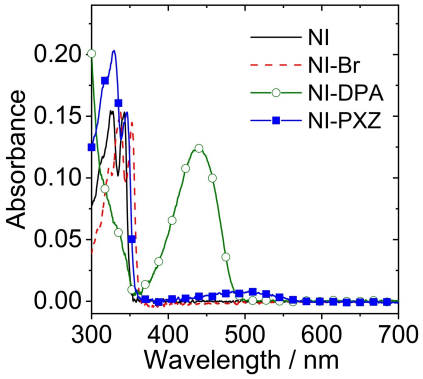

Figure 2. UV/Vis absorption spectra of **NI**, **NI-Br**, **NI-DPA** and **NI-PXZ** in *n*-hexane. $c = 1.0 \times 10^{-5}$ M, 25° C.

Single crystals of **NI-PXZ** were obtained by slow diffusion of *n*-hexane (HEX) into a dichloromethane (DCM) solution of the compound. X-ray diffraction shows that the dihedral angle between the NI and PXZ units is 83.5° (Figure 1). The PXZ unit adopts a planar geometry, differently from PTZ, which has a puckered geometry.[25] The detailed parameters and the molecular structure of **NI-PXZ** are presented in Table S1 in the Supporting Information.

UV/Vis absorption spectroscopy

In order to study the coupling of the compounds in the ground state, we first measured the UV/Vis absorption spectrum (Figure 2). **NI** shows a typical structured absorption band in the 300–350 nm range. A similar spectrum was observed for **NI-Br**. For **NI-PXZ**, a weak, broad and structureless band was observed in the range 360–560 nm, centered at ca. 500 nm. This band is attributed to the charge transfer (CT) absorption, as the result of electronic coupling between the PXZ and the NI moieties.[16a,26] We conclude that the coupling is weak, since the structured absorption band in the range of 300–350 nm is similar to that of **NI**. Geometry optimization at DFT level indicates that **NI-PXZ** adopts an orthogonal geometry (see later section). The molecular structure determined by the single crystal X-ray diffraction (Figure 1) also supports this observation (the dihedral angel between the NI and PXZ moieties is 83.5°).

In case of **NI-DPA**, the π-conjugation between the amine and the NI moieties is more significant, and as a result, an intense CT absorption band centered at 440 nm is observed, while the structured absorption in the 300–350 nm range is lacking.[26a] The CT absorption band of **NI-PXZ** (centered at 496 nm) is slightly red-shifted as compared to the previously reported analogue of **NI-PTZ** dyad (the CT band was centered at 450 nm).[16a] The absorption properties of the compounds are summarized in Table 1.

The transition dipole moments M_{abs} of the $S_0 \rightarrow {}^1$CT transition and the electronic coupling matrix elements V_{DA} of the S_0 and the Franck-Condon ^{1}CT states were calculated based on the CT absorption band with Equations (1) and (2) (See Supporting Information for the detail of the equations):

Table 1. Absorption properties and electronic coupling matrix elements (V_{DA}) of the compounds.[a]

	λ_{abs} ($S_0 \rightarrow$LE) [nm/eV][b]	λ_{abs} ($S_0 \rightarrow$CT) [nm/eV][b]	M_{abs} ($S_0 \rightarrow$CT) [D][c]	$\Delta\mu_{12}$ [D][d]	V_{DA} [eV][e]
NI-PXZ	330/3.76	496/2.50	1.03	2.17	0.142
NI-DPA	289/4.29	440/2.82	3.57	7.18	0.463

[a] In *n*-hexane. [b] These maxima of the $S_0 \rightarrow {}^1$LE band and the $S_0 \rightarrow {}^1$CT band were obtained by experiments. [c] Transition dipole moments of $S_0 \rightarrow {}^1$CT transitions. [d] Dipole-moment change between ground and excited electronic states obtained from DFT calculations. [e] Electronic coupling matrix element between S_0 state and ^{1}CT state.

$$|M_{abs}|^2 = \frac{3\ln 10}{8\pi^3 N_A}\frac{hc}{n\tilde{\nu}_{CT}}\int_{band}\varepsilon(\tilde{\nu}_{CT})d\tilde{\nu} \quad (1)$$

$$V_{DA}(cm^{-1}) = \left(\frac{2.06\times10^{-2}}{R}\right)\left(\varepsilon^{CT}_{max}\tilde{\nu}^{CT}_{max}\Delta\tilde{\nu}^{CT}_{1/2}\right)^{1/2} \quad (2)$$

The V_{DA} for **NI-PXZ** was estimated as $V_{DA}=0.142$ eV (Table 1), which is comparatively larger than the previously reported value for the **NI-PTZ** analogue (0.110 eV).[16a] It shows that the CT state has a stronger coupling with the ground state in **NI-PXZ**. This is reasonable, since in the absorption spectrum, the $S_0\rightarrow{}^1$CT transition band of **NI-PXZ** is wider than that of **NI-PTZ**. From the single crystal structure, the dihedral angle of **NI-PXZ** is 83.5°, which will induce slightly stronger coupling at ground state (the dihedral angle of **NI-PTZ** is 84.9°). Similarly, **NI-DPA** has a more significant π-conjugation effect, therefore the coupling is stronger in **NI-DPA**, the V_{DA} value is 0.463 eV (Table 1).

Thermally activated delayed fluorescence (TADF) and luminescence property

For the molecules of the D–A system, the solvent-dependent fluorescence spectrum can directly demonstrate the existence of intramolecular charge transfer (ICT). The fluorescence spectra of the compounds are reported in Figure 3. As compared to **NI-DPA**, the fluorescence of **NI-PXZ** is significantly quenched (Figure 3a), as observed for the previously reported analogue dyad **NI-PTZ**.[16a] The fluorescence intensity and emission wavelength is highly dependent on the solvent polarity (see Figure 3b), with strong quenching in polar solvents. In comparison, the solvent polarity-dependence for **NI-DPA** is weaker (Figure 3c). The photophysical property of the compounds is summarized in Table 2.

Note in *n*-hexane, the fluorescence emission of **NI-PXZ** (centered as 582 nm, Table 2) is red-shifted as compared to **NI-DPA** (centered at 495 nm, Table 2). Both emission bands are broad and structureless, indicating the CT character of the emissive state. **NI-PXZ** shows a broad, weaker emission band in toluene (TOL), and the fluorescence is quenched in other solvents with higher polarity, indicating that the emissive state has significant CT character. The difference with **NI-DPA** may be due to the restricted orthogonal geometry of **NI-PXZ**.

The fluorescence excitation spectra and the UV/Vis absorption spectra of the compounds are compared (Figure S12). For **NI-PXZ**, with normalization at the CT absorption band position, the two spectra show similar magnitude in the LE absorption region (Figure S12a in the Supporting Information). For **NI-DPA**, the CS yield upon photoexcitation into the higher excited state is lower than photoexcitation into the CT absorption band (Figure S12b in the Supporting Information), which is caused by other non-radiative decay of the upper singlet excited state, such as ISC (Table 3).

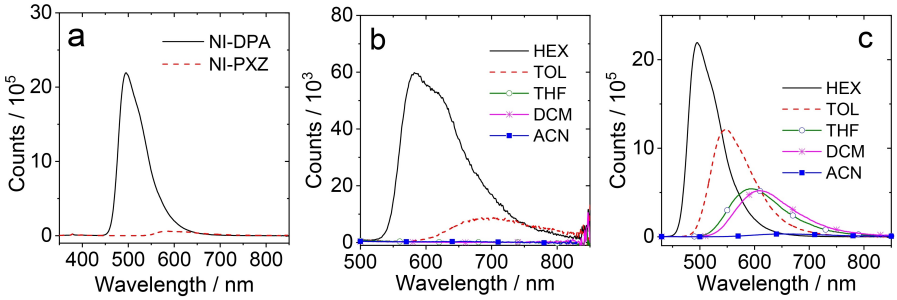

Figure 3. (a) Comparison of the fluorescence spectra of **NI-PXZ** and **NI-DPA** in *n*-hexane. Fluorescence emission spectra of (b) **NI-PXZ** and (c) **NI-DPA** in different solvents. Optically matched solutions were used ($A=0.100$ at $\lambda_{ex}=340$ nm), 25 °C.

Table 2. Photophysical properties of the compounds.

	λ_{abs}[a] [nm]	ε[b]	λ_{em}[c] [nm]	τ_T[d] [μs]	τ_F[e] [ns]	τ_F[f] [ns]	τ_P[g] [ms]	Φ_Δ[h] (%)	E_T[i] [eV]	Φ_F[j] (%)
NI	325	1.55	365	67.2	3.7	6.6	440	14	2.29	0.520
NI-Br	338	1.54	378	122	3.7	6.5	8.42	16	2.24	0.440
NI-PXZ	330[k]/496[l]	2.04[k]/0.09[l]	582	15.4[m]	8.4/297.2[n]	16.4/17.0 × 10^3[n]	-[o]	7	-[o]	3.82
NI-DPA	440[l]	1.24[l]	495	95.3[m]	10.2	14.4	-[o]	5	-[o]	75.2

[a] Maximal UV/Vis absorption wavelength in *n*-hexane (1.0×10^{-5} M). [b] Molar absorption coefficient absorption maxima, ε: 10^4 M^{-1} cm^{-1}. [c] Maximal fluorescence wavelength in *n*-hexane. [d] Intrinsic triplet lifetime in *n*-hexane eliminates the self-quenching effect of TTA (see Supporting Information for details). [e] Fluorescence lifetime in *n*-hexane under air atmosphere at 298 K. [f] Fluorescence lifetime in *n*-hexane under N_2 atmosphere at 298 K. [g] Phosphorescence lifetime in 2-methyltetrahydrofuran under N_2 atmosphere at 77 K. [h] Singlet oxygen quantum yield ($^1O_2$) ($\lambda_{ex}=310$ nm) with $Ru(bpy)_3[PF_6]_2$ as standard ($\Phi_\Delta=0.57$ in DCM) in *n*-hexane. [i] Triplet energy levels at 77 K calculated using low-temperature phosphorescence emission wavelength, $E_T=1240/\lambda_{em}$. [j] Absolute fluorescence quantum yields, determined with optical integration sphere. [k] The transition of $S_0\rightarrow{}^1$LE. [l] The transition of $S_0\rightarrow{}^1$CT. [m] No need to consider the TTA effect because of the low triplet quantum yield or short triplet lifetime. [n] Thermally activated delayed fluorescence lifetime under N_2 atmosphere at room temperature. [o] Not observed.

In order to study the possible TADF properties of **NI-PXZ**, we recorded the luminescence of the compounds under N_2 and air atmosphere (Figure 4).[27] For **NI**, a structured emission band in the range of 350–500 nm was observed, which is attributed to the fluorescence.[19b] The emission intensity is quenched to large extent in aerated solution. Similar results were observed for **NI-Br**. A red-shifted emission band in the 550–700 nm range was also observed for **NI-Br**, assigned to the phosphorescence (The T_1 state energy is approximated as 2.25 eV).[19b] This assignment is supported by the long luminescence lifetime (130 μs, the luminescence decay trace was monitored at 580 nm. Figure S26b in the Supporting Information). In comparison the luminescence lifetime of **NI-Br** monitored at 380 nm in deaerated solution is 0.2 ns (86.2%)/6.5 ns (13.8%) (Figure S26a in the Supporting Information). We also measured the phosphorescence of **NI-Br** at 77 K (Figure S30 in the Supporting Information), observing a structured emission band in the 550–700 nm range, with lifetime of 8.42 ms.

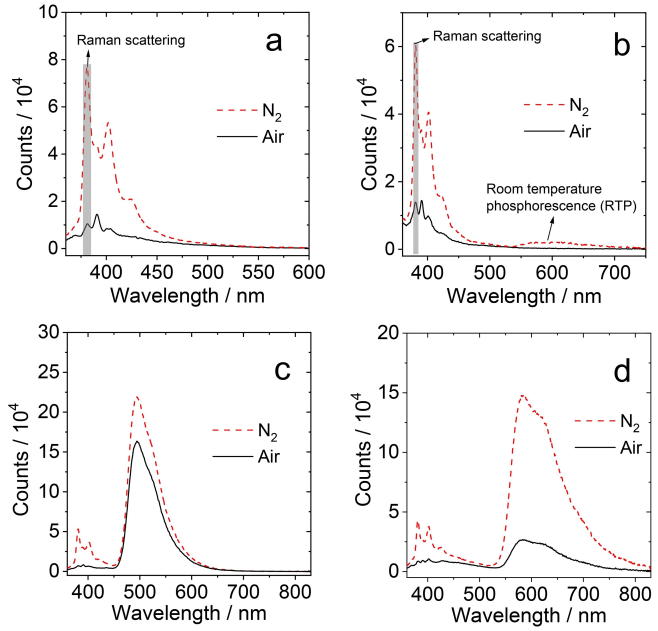

Figure 4. Fluorescence spectra of (a) **NI**; (b) **NI-Br** ;(c) **NI-DPA** and (d) **NI-PXZ** in *n*-hexane, $c = 1.0 \times 10^{-5}$ M, $\lambda_{ex} = 340$ nm, 25 °C.

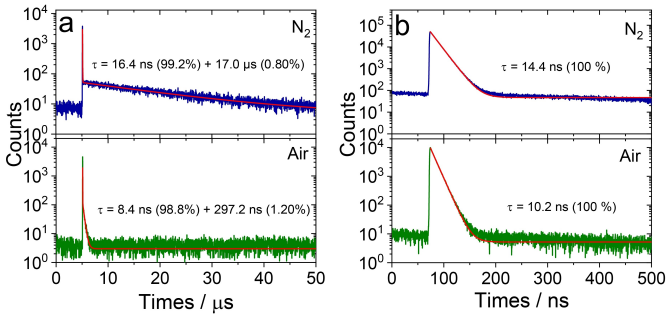

Figure 5. Fluorescence decay traces of **NI-PXZ** and **NI-DPA** under different atmospheres (N_2, Air). (a) **NI-PXZ**. $\lambda_{ex} = 340$ nm, decay trace at 580 nm. (b) **NI-DPA**. $\lambda_{ex} = 340$ nm, decay trace at 480 nm, excited with nanosecond EPLED (340 nm). $c = 1.0 \times 10^{-5}$ M in *n*-hexane, 25 °C.

For **NI-DPA**, a similar LE fluorescence band was observed in the range 350–450 nm (Figure 4c), together with a more intense broad emission band in the 450–650 nm range, which is attributed to a CT emission.[28] The luminescence lifetimes monitored at the two emission bands were determined as 3.4 ns and 10.4 ns, respectively (Table 2 and Figure S27 in the Supporting Information). For **NI-PXZ**, a similar LE emission band was observed in the 350–500 nm range (Figure 4d). Interestingly, the CT emission band is centered at 582 nm, which is red-shifted by 3020 cm^{-1} as compared to that of **NI-DPA**. We assign this difference to the more significant CT character of the emissive S_1 state in **NI-PXZ**.

Interestingly, a long-lived luminescence was observed for **NI-PXZ** under N_2 atmosphere (Figure 5a). The fluorescence decay of **NI-PXZ** monitored at 580 nm has a distinct biexponential behavior, with a fast decaying component with lifetime of 16.4 ns (99.2%) and a slow decay component with lifetime of 17.0 μs (0.80%), which we attribute to TADF.[27] Notably the slow decaying component has a much longer lifetime than the previously reported analogue **NI-PTZ** (2.60 μs, 3.40%).[16a] This lifetime is also longer compared with a recently reported analogue derived from aniline (1.20 μs), instead of *n*-butylamine.[24a] Although the long-lived component has a small weight, we believe it is not an artifact, since the fluorescence intensity is quenched under air atmosphere and the luminescence lifetimes are reduced to 8.4 ns (98.8%)/297.2 ns (1.20%) (Figure 5a). In comparison, **NI-DPA** shows a normal fluorescence lifetime of 14.4 ns in deaerated solution and 10.2 ns in aerated solution, and in both cases the decay is mono-exponential (Figure 5b). As the temperature decreases from 298 to 178 K, the emission intensity of **NI-PXZ** at 580 nm gradually decreases (Figure S24a in the Supporting Information). This anomalous observation is explained if considering that decreasing the temperature, the environmental thermal energy decreases and reduce the driving force required for the reversed ISC (rISC) necessary for TADF. This change is opposite compared to what observed for normal luminescent materials. For example, the luminescence of **NI**, **NI-Br** and **NI-DPA** increases as the temperature decreases, since at low temperatures non-radiative transitions are reduced because of the decreased vibrational mobility, enhancing the radiative transition channel (Figure S24 in the Supporting Information). We also observed TADF in cyclohexane (Figure S28 in the Supporting Information). However, no TADF was observed for **NI-PXZ** in toluene and other polar solvents (Figure S13-S16 in the Supporting Information).

As a preliminary evaluation of the ISC of the compounds, we measured their singlet oxygen quantum yields (Φ_Δ). It is known that **NI** and **NI-Br** have efficient ISC. For the former, the ISC is due to the $S_1 \rightarrow T_4$ transition.[29] Moderate singlet oxygen quantum yields were observed for **NI** and **NI-Br** (Table 3), with Φ_Δ values not substantially sensitive to solvent polarity (see Table 3). For **NI-PXZ**, the Φ_Δ values are much smaller and highly sensitive to the solvent polarity: no $^1O_2$ was observed in polar solvents such as THF, DCM and ACN. Inhibition of ISC in polar solvents indicates that another efficient non-radiative decay

Table 3. Singlet oxygen quantum (Φ_Δ) yields of derivatives in different solvents.

	HEX[d]	TOL[e]	THF[f]	DCM[g]	ACN[h]
NI-PXZ	32[a]/ 7[c]	7[a]/ 1[c]	–[i]	–[i]	–[i]
NI-DPA	41[b]/ 5[c]	87[b]/ 21[c]	18[b]/ 20[c]	68[b]/ 17[c]	6[b]/ 9[c]
NI-Br[c]	16	20	30	49	48
NI[c]	14	16	24	37	57

[a] λ_{ex} = 500 nm. 2,6-didiiodoBodipy was used as standard compound, Φ_Δ = 85% in TOL. [b] λ_{ex} = 450 nm. $[Ru(bpy)_3]^{2+}$ was used as standard compound, Φ_Δ = 57% in DCM. [c] λ_{ex} = 330 nm. $[Ru(bpy)_3]^{2+}$ was used as standard compound, Φ_Δ = 57% in DCM. [d] $E_T(30)$ = 30.9 kcal/mol, [e] $E_T(30)$ = 33.9 kcal/mol, [f] Tetrahydrofuran, $E_T(30)$ = 37.4 kcal/mol. [g] Dichloromethane, $E_T(30)$ = 41.1 kcal/mol. [h] Acetonitrile, $E_T(30)$ = 46.0 kcal/mol. [i] Not observed.

channel exists for the ^{1}CS state, such as fast CR to the ground state.[30] The solvent dependence of ISC is typical in case of SOCT-ISC.[12c,14d,f–h]

Electrochemical and spectroelectrochemical study of the compounds

We demonstrate the existence of ^{1}CS states in steady-state absorption and emission spectra. In order to determine the energy of CS state and to have an in-depth understanding of the photophysics of the dyad, its electrochemistry was analyzed (Figure 6). Although the oxidation potential of the native PXZ (+0.22 V vs. Fc/Fc$^+$) is lower than that of PTZ (+0.30 V vs. Fc/Fc$^+$),[22a,23] the first reversible oxidation wave of the **NI-PXZ** was observed at +0.43 V, which is higher compared to that of the previously reported analogue **NI-PTZ** (+0.39 V).[16a]

The Gibbs free energy changes (ΔG_{CS}) for charge separation (CS) as well as the energy of the charge separated states were calculated using the Weller equation (Equations (3)–(5)). See Supporting Information for the detail of the equations) and the obtained values are listed in Table 4:

$$\Delta G_{CS} = e[E_{OX} - E_{RED}] - E_{00} + \Delta G_S \quad (3)$$

$$\Delta G_S = -\frac{e^2}{4\pi\varepsilon_s\varepsilon_0 R_{CC}} - \frac{e^2}{8\pi\varepsilon_0}\left(\frac{1}{R_D}+\frac{1}{R_A}\right)\left(\frac{1}{\varepsilon_{REF}}-\frac{1}{\varepsilon_S}\right) \quad (4)$$

$$E_{CS} = e[E_{OX} - E_{RED}] + \Delta G_S \quad (5)$$

The obtained ΔG_{CS} indicate that charge separation is thermodynamically allowed even in non-polar solvent such as HEX (in agreement with the fs-TA spectra, see later section). Moreover, the calculated CS state energy is less than 2.30 eV, especially in polar solvents. These results indicate that the CS state energy is lower than that of the ^{3}LE state of the NI moiety (2.29 eV),[20] as confirmed by the nanosecond transient absorp-

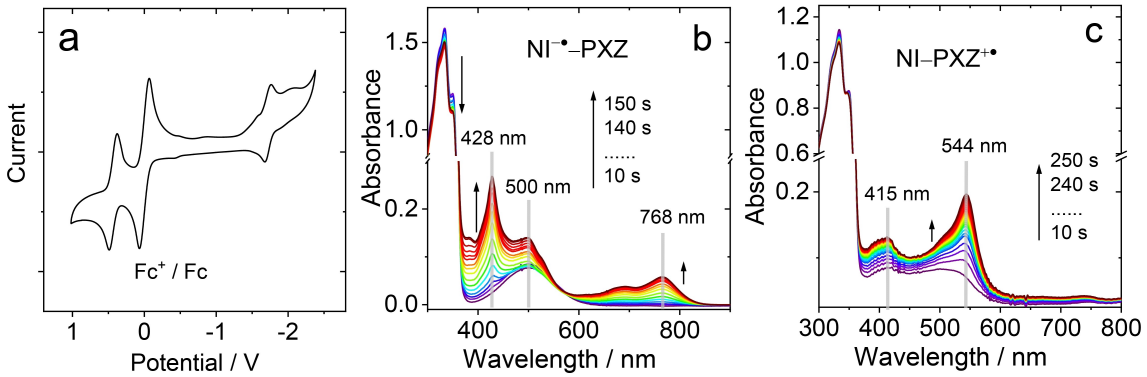

Figure 6. (a) Cyclic voltammograms of **NI-PXZ** in deaerated DCM, 0.10 M Bu_4NPF_6 was used as the supporting electrolyte and $Ag/AgNO_3$ was used as the reference electrode. Scan rates: 50 mV s^{-1}. Ferrocene (Fc) was used as an internal reference. Spectroelectrochemistry study of the dyad, i.e. the evolution of the UV/Vis absorption of **NI-PXZ** upon (b) reduction with an applied potential of −1.79 V and (c) oxidation with an applied potential of +0.54 V on the working electrode. $Ag/AgNO_3$ was used as reference electrode. The spectra were recorded in situ with a spectroelectrochemical cuvette (1 mm optical path). $c = 3.0\times10^{-4}$ M in deaerated DCM. 20 °C.

Table 4. Redox Potentials of **NI-PXZ** and Driving Forces of Charge Separation (ΔG_{CS}) and the Energy of Charge Separated State (CSS) for NI Derivatives in Different Solvents.

	E_{OX} [V]	E_{RED} [V]	ΔG_{CS} [eV] HEX	E_{CSS} [eV] TOL	DCM	ACN	HEX	TOL	DCM	ACN
NI-PXZ[a]	+0.43	−1.72	−1.23	−1.36	−1.67	−1.69	2.28/2.26[b]	2.16/2.13[b]	1.85/–[c]	1.83/–[c]

[a] E_{00} = 3.52 eV. E_{00} is the energy level of singlet excited state localized on NI moiety (^{1}NI*) approximated with the crossing point of UV/Vis absorption and fluorescence emission spectra. [b] The *E*css value obtained from the experimental value: *E*css = 1240/λ_{00} (λ_{00} is the intersection of CT absorption spectrum and CT emission spectrum. In nm). [c] Due to the extremely weak emission, the calculation was not carried out.

tion spectral studies (see later section). The low-lying CS states may be responsible for low ISC yields observed for **NI-PXZ** in polar solvents. For **NI-DPA**, the ^{3}LE state has an energy of ca. 2.10 eV, as estimated by TDDFT calculations.

Furthermore we performed a spectroelectrochemical investigation, in order to analyze the absorption features of the radical anion and cation of **NI-PXZ** and to facilitate the assignment of the absorption bands in the femtosecond and nanosecond transient absorption spectra. When applying a negative potential, the absorption band of the NI moiety in **NI-PXZ** centered at 330 nm decreased, and new absorption bands at 428 nm and 500 nm developed, as well as a weaker broad band in the range 600–850 nm (Figure 6b). These features are attributed to the NI radical anion ($NI^{-\bullet}$).[16a,31] With a positive potential applied, a new absorption band centered at 544 nm was observed (Figure 6c), which is assigned to the absorption of the PXZ radical cation ($PXZ^{+\bullet}$).[26c] Note that these absorption bands may be slightly different from what would be observed for the CT state of **NI-PXZ**, because in the spectroelectrochemical studies the $PXZ^{+\bullet}$ and $NI^{-\bullet}$ do not exist *simultaneously*, while in the CT state, they do, and the interaction between the radical anion and cation could induce a variation or shift of these bands. This is different from the scenario of the electron donor-acceptor dyads containing long linkers.[32] Based on the above results, we can assign the following species observed in the femtosecond and nanosecond transient absorption spectra.

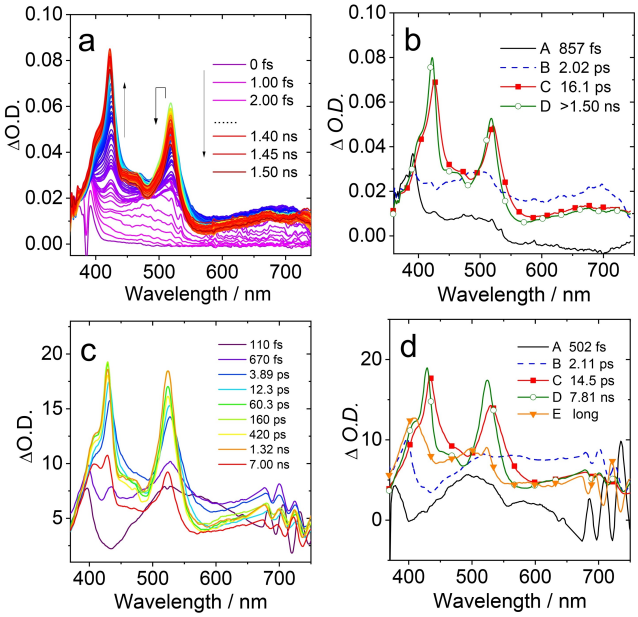

Figure 7. Femtosecond transient absorption spectra of **NI-PXZ**. (a) Transient absorption spectra and (b) relative EADS obtained with global analysis in *n*-hexane. (c) Transient absorption spectra of **NI-PXZ** with longer time windows, 7 ns and (d) relative EADS obtained with global analysis, the raw data are reported in (c). Excited at 340 nm.

Femtosecond transient absorption spectra

In order to study charge separation, charge recombination and the ISC in **NI-PXZ**, femtosecond transient absorption (fs-TA) spectra were recorded (Figure 7 and Figure S32-S35 in the Supporting Information). The transient absorption spectra of **NI** measured in *n*-hexane and the evolution associated difference spectra (EADS), obtained by a sequential global analysis, are presented in Figure S32. At early delay times after pulsed laser excitation, a positive narrow band centered at 380 nm and a broader positive band centered at 480 nm were observed. These bands are assigned to the excited state absorption (ESA) of the S_1 state of **NI**.[31,33] After 1.31 ps, the spectral intensity slightly increases, and the bands slightly narrow, because of the vibrational relaxation of the ^{1}NI* state (blue line). After 11.5 ps the spectral shape changes significantly: the ESA bands centered at 380 nm and 480 nm recover, while a new structured band with two peaks at 430 nm and 460 nm (red, EADS) emerges. According to previous studies, this latter band can be assigned to a triplet state formed via the ISC ($S_1 \rightarrow T_4$). The ISC rate (11.5 ps) is in good agreement with the previously reported values obtained with gas phase picosecond time- and frequency-resolved multiphoton ionization spectroscopy (10–20 ps).[29] The triplet state decays with a time constant longer than the time interval of our measurement ($>$1.5 ns). Nanosecond transient absorption spectra indicate the triplet state lifetime in deaerated solution is 67.2 μs (Figure S37 in the Supporting Information).

The spectral evolution of **NI-Br** is very similar to that of **NI** (Figure S32d in the Supporting Information). Upon pulsed laser excitation, we observed a broad band centered at 500 nm, assigned as the ESA band of the S_1 state (black line of Figure S32d in the Supporting Information). The intensity of this band decreases after few picoseconds, while the features typical for the triplet state emerge after only 6.63 ps.[16a] The ISC rate for **NI-Br** is slightly smaller as compared to **NI**. The triplet state lifetime of **NI-Br** was determined as 122 μs with nanosecond transient absorption spectra (Figure S39 in the Supporting Information).

The pump probe spectra of **NI-PXZ** measured in *n*-hexane are reported in Figure 7, together with the EADS obtained from global analysis. The first EADS (black line in Figure 7b) can be recognized as a localized singlet excited state of ^{1}NI* by comparison with the spectra reported in Figure S32. The spectrum rapidly changes, and in the second spectral component, rising within 857 fs, a very broad absorption band is observed, (blue line, Figure 7b). Considering the very fast kinetics, this spectral evolution can be interpreted in terms of a relaxation of the ^{1}NI* state, however the rise of intensity in the 600–750 nm spectral region may suggest that part of the population is evolving towards a CT state.

In about 2.02 ps, the transient spectrum evolves significantly, with the appearance of two intense sharp bands, peaked at 427 nm and 520 nm together with a broad absorption band in the range of 600–750 nm. Comparison with spectroelectrochemical data allows to assign the band at 427 nm and the broad feature at $>$600 nm to the $NI^{-\bullet}$ anion,[31,34] while the narrow band centered at 520 nm to the $PXZ^{+\bullet}$ cation.[26c,35] The

appearance of these bands confirms the occurrence of electron transfer from PXZ to the NI moiety. Within 16.1 ps the intensity of the two bands increases and both peaks blue shifts by about 5 nm, indicating a vibrational relaxation of the charge separated (CS) state. Charge recombination cannot be observed within 1.5 ns, therefore we used a femtosecond transient absorption spectrometer with a larger time window to further analyze the time evolution of the dyad (Figure 7c and 7d).

Measurements performed on the extended time window indicate that the band at 520 nm appears to decay faster as compared to that at 420 nm. This spectral change indicates the evolution towards the triplet state, which, according to nanosecond transient spectroscopy, presents an ESA band centered at 430 nm, but no peaks at 520 nm. The data recorded up to 7 ns have been analyzed using five kinetic constants, and the fifth EADS has been added to improve the fit. The initial time constants obtained by analyzing the data sets recorded on the 1.5 ns and 7 ns timescales are in reasonable agreement. The measurements executed up to 7 ns allows a better estimate of the time constants at longer pump-probe delays. The final spectral component observed for **NI-PXZ** (orange line in Figure 7d) can be interpreted as a CS state mixed with the ^{3}LE, since absorption features of ^{3}NI* can be recognized in the spectrum, in good agreement with the ns-TA measurements. This result indicates that triplet features start to appear within 7.81 ns, although signatures attributable to the CS state are still visible on this timescale. Bands attributable to the CS state are also visible on a longer timescale, as confirmed by ns transient absorption spectroscopy. Considering that the lifetime of the state probed with ns-TA is 15.4 μs, we propose that the long-lived CS state has a triplet spin multiplicity, and that the ^{3}CS forms with the NI-localized ^{3}LE state as the precursor.

The CS and CR of **NI-PXZ** in toluene and acetonitrile were also studied (Figure S34 in the Supporting Information). In toluene, some residual signal is persistent within the time window analyzed with femtosecond transient absorption spectroscopy, whose spectral shape is similar to the species observed in ns-TA spectra (see next section). We propose that also in this case the long-lived CS state is a ^{3}CS state, not ^{1}CS state. This assignment is supported by the observation that the luminescence lifetime of the CS state in toluene is about 2.50 ns: this value is close to the lifetime of 1.83 ns obtained for the third component from global analysis, indicating that the third component is attributable to ^{1}CS, while the long-lived CS state is likely to be a triplet state. Therefore, due to solvation in toluene and more polar solvents, a very fast charge separation process of ^{3}LE→^{3}CS may occur, so it is too fast to observe the signal of ^{3}LE while, only the signals of ^{1}CS and ^{3}CS are observed (please note that in the compact electron-donor-acceptor system, RP-ISC is difficult to happen). ^{1}CS→^{3}LE ISC time constants in toluene is 1.83 ns. We speculate that in acetonitrile, most of the ^{1}CT state undergoes charge recombination in 10.3 ps and given the small residual signal on the long timescale, we are unable to estimate the ^{1}CT to ^{3}LE rate.

We also measured the pump-probe spectra of the **NI-DPA** (Figure S33 in the Supporting Information). We did not observe a triplet state with mixed CS/LE character.

The CS and CR processes were simulated using the Marcus equation under simplifying assumptions (Equation (6), see Supporting Information for details of the formula). In Figure 8a the electron transfer rates in different solvents (HEX, TOL and ACN) are reported as a function of $\Delta G_{ET.}$[30a] The ΔG_{ET} of charge separation is obtained from electrochemical data, while that of charge recombination is calculated from the formula $\Delta G_{CR} = -(\Delta G_{CS} + E_{00})$, where E_{00} is the energy level of singlet excited state localized on NI moiety (^{1}NI*), approximated with the crossing point between UV/Vis absorption and fluorescence emission spectra. The electron transfer rate is obtained from fs-TA data.

By fitting the experimental data points, the total reorganization energies (λ) and electronic coupling matrix elements (V) for **NI-PXZ** are estimated as 1.24 eV and 50.8 cm^{-1}, respectively. We observe that the CS process for **NI-PXZ** in different solvents is located in the Marcus normal region, whereas the CR is in the Marcus inverted region (Figure 8a).

$$k_{ET} = \left(\frac{4\pi^3}{h^2 \lambda k_B T}\right)^{1/2} V^2 exp\left[-\frac{(\Delta G_{ET} + \lambda)^2}{4\lambda k_B T}\right] \quad (6)$$

$$k_B T \ln k_{ET} + \frac{\Delta G_{ET}}{2} = k_B T \ln\left[\left(\frac{4\pi^3}{h^2 \lambda k_B T}\right)^{1/2} V^2\right] - \frac{\lambda}{4} - \frac{(\Delta G_{ET})^2}{4\lambda} \quad (7)$$

We analyzed the dependence of the driving force on the rate constant through Equation (6), which can be transformed into the linear expression shown in Equation (7). Plots of [k_BT ln k_{ET}+(ΔG_{ET}/2)] versus (ΔG_{ET})^2 for electron transfer give a linear correlation for **NI-PXZ**, as shown in Figure 9b, from which we can estimate λ and V for **NI-PXZ** to be 1.19 eV and 61.5 cm^{-1}.

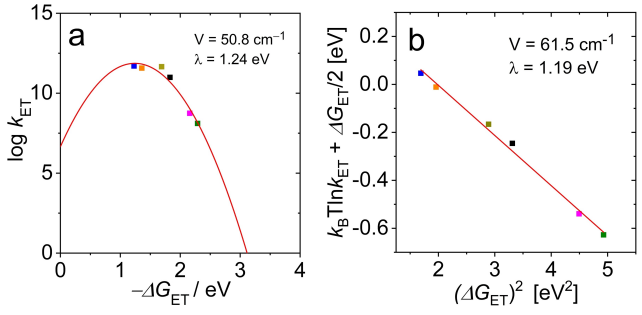

Figure 8. (a) Plot of intramolecular electron-transfer rate constants in **NI-PXZ** vs. the thermodynamic driving force (-ΔG_{ET}). The red line represents the best fit with Equation (6), which gives the reorganization energy λ = 1.24 eV and electronic coupling matrix elements V = 50.8 cm^{-1}. (b) Plot of [k_BT ln k_{ET} + (ΔG_{ET}/2)] vs. (ΔG_{ET})^2 for **NI-PXZ** and fit with Equation (7), which gives λ = 1.19 eV and V = 61.5 cm^{-1}). The data used are CS data in HEX (blue point), CS data in TOL (orange point), CS data in ACN (brown point), CR data in HEX (black point), CR data in TOL (magenta point) and CR data in ACN (olive point), respectively.

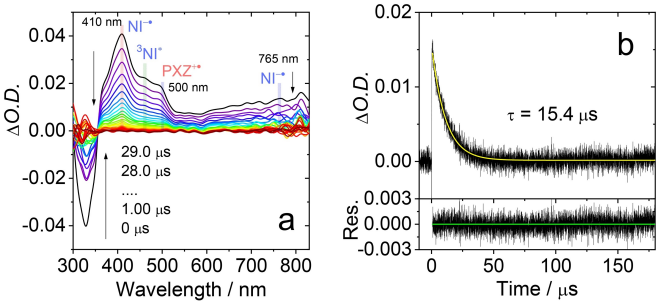

Figure 9. Nanosecond transient absorption spectra of the dyads. (a) Transient absorption spectra of **NI-PXZ**, $c = 3.0 \times 10^{-5}$ M and (b) decay curves at 410 nm after pulsed laser excitation at 355 nm, $c = 1.0 \times 10^{-5}$ M in *n*-hexane. 25 °C.

Nanosecond transient absorption spectra

To study the transient species formed with **NI-PXZ** upon photoexcitation, we studied the nanosecond transient absorption (ns-TA) spectra of the compounds. The ns-TA spectra of **NI-PXZ** measured in *n*-hexane are presented in Figure 9. Upon nanosecond pulsed laser excitation, positive band centered at 410 nm was observed, which is not the characteristic ESA band of the ^{3}NI state, expected at 470 nm.[16a,36] Considering that the absorption of NI$^{-\bullet}$ was determined at ca. 430 nm in a **NI-PTZ** dyad,[16a,36a,c] the positive absorption band observed in the ns-TA spectrum appears more similar to that of NI$^{-\bullet}$ (refer to the spectroelectrochemical study, Figure 6), other than to that of ^{3}NI state.[16a,36a] Similar ns-TA spectra were observed in cyclohexane (CHX. Figure 10). In aerated *n*-hexane (HEX) solution the ESA features of **NI-PXZ** do not change, but the lifetime is reduced to 38.2 ns (4.30 %)/258 ns (95.7 %) (the trace follows a biexponential decay, see Figure S36 in the Supporting Information). Previously it was found that the lifetime of a ^{3}CS state can be shortened by O_2,[37] which lead us to propose that the state populated upon pulse laser excitation has significant CS character.

The excited state lifetime of **NI-PXZ** was determined 15.4 µs (in HEX), a smaller value as compared to that of **NI-Br** (Figure S39 in the Supporting Information, 30.0 µs–157 µs for previous result).[16a,31] Also the spectral shape is different compared to both **NI-Br** and **NI**. The reference compounds indeed present absorption bands peaked at 370 nm and 480 nm (**NI-Br**), and 460 nm (**NI**) but no weak, broad absorption band in the range of 600–800 nm. The intrinsic triplet state lifetime was determined as 122 µs for **NI-Br**. The triplet state lifetime of **NI** was determined as 58.9 µs in ACN (1.0×10^{-5} M, Figure S38 in the Supporting Information), much longer than the previous result of 9 µs.[20] These results support the statement that the transient absorption observed for **NI-PXZ** is not an ordinary ^{3}NI state, rather, it involves ^{3}CS state, because the TADF luminescence lifetime show that the ^{1}CS is short-lived (16.4 ns. Figure 5).

In order to further investigate the ns-TA spectra of **NI-PXZ**, measurements were repeated in solvents with different polarity (Figure 10). In CHX, as in HEX, a broad absorption band in the 400–550 nm range was observed, similar to the NI$^{-\bullet}$ absorption. The lifetime of **NI-PXZ** in CHX is 24.0 µs, (Figure 10. $E_T(30) =$ 30.9 kcal/mol for cyclohexane) slightly longer than that in HEX (15.4 µs. $E_T(30) = 31.0$ kcal/mol). Interestingly, in TOL ($E_T(30) =$ 33.9 kcal/mol), a distinct absorption band centered at 530 nm was observed, along with the sharp, strong absorption band centered at 430 nm. The former band is distinctive for PXZ$^{+\bullet}$. The lifetime of the transient species is much shorter (675 ns. Figure 10f), and the ^{3}NI contribution is less significant. Note that

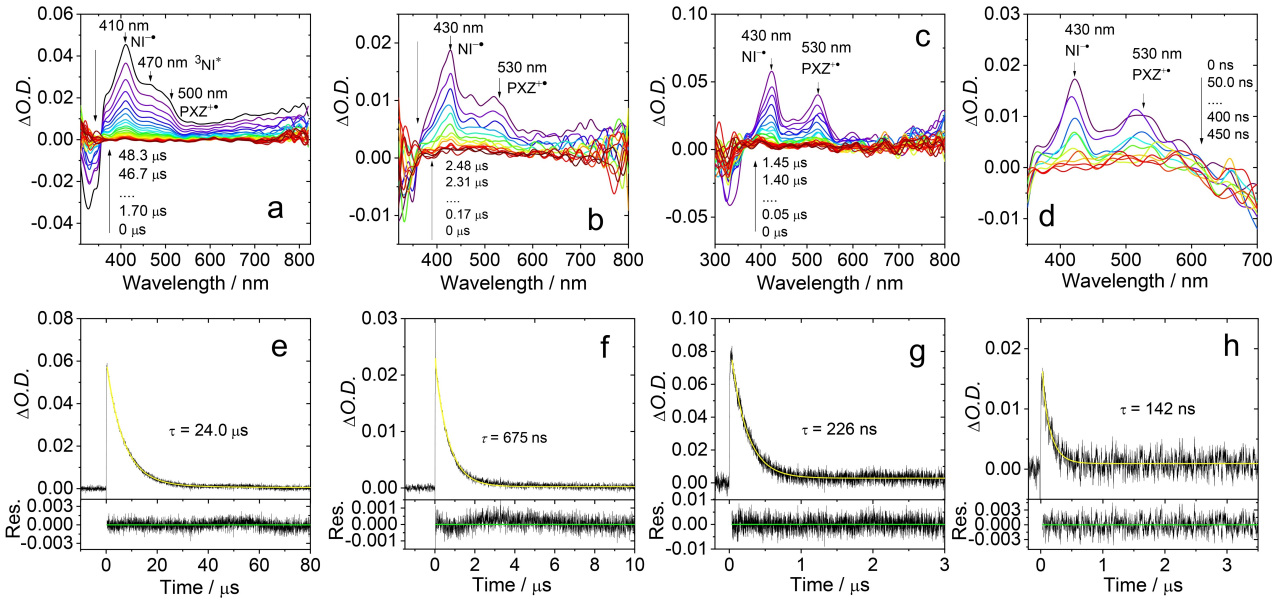

Figure 10. Nanosecond transient absorption spectra of **NI-PXZ** in (a) cyclohexane, (b) toluene, (c) tetrahydrofuran and (d) acetonitrile, $c = 3.0 \times 10^{-5}$ M and decay curves at 420 nm in (e) cyclohexane, (f) toluene, (g) tetrahydrofuran and (h) acetonitrile after pulsed laser excitation at 355 nm, $c = 1.0 \times 10^{-5}$ M, 25 °C.

no TADF was observed for **NI-PXZ** in toluene. It is known that the rISC of ^{3}CS→^{1}CS in TADF is mediated by the ^{3}LE state, and that direct ^{3}CS→^{1}CS is forbidden.[18c,d] Since the lifetimes determined by monitoring the decay at three representative wavelengths are close, and considering the short lifetime of the ^{1}CS state, we propose that the state we observed in the ns-TA spectra is the ^{3}CS state. This is reasonable in compact electron donor-acceptor dyads, where the electron exchange energy (*J*) is large. Moreover, the ^{3}NI* state energy should be very close to the ^{3}CS state in HEX, whereas it may become higher than the ^{3}CS state in polar solvents, where the energy of CS states decreases.

In THF (Figure 10c), two distinct absorption bands centered at 430 nm and 530 nm were observed, which are attributed to $NI^{-\bullet}$ and $PXZ^{+\bullet}$, respectively (refer to Figure 7). No LE triplet state signal was observed. The transient species has lifetime of 226 ns, which is shorter than that in TOL (675 ns). Similar results were observed in ACN (Figure 10d), where the measured CS state lifetime is much shorter (142 ns). To the best of our knowledge, these CS lifetimes are long, considering that the dyads present a donor and acceptor directly connected.[12]

On the contrary, no significant solvent polarity-dependency for the triplet state lifetime was observed for **NI** and **NI-Br** (τ_T= 67.2 μs of **NI** in HEX, τ_T=58.9 μs of **NI** in ACN, τ_T=122 μs of **NI-Br** in HEX, τ_T=101 μs of **NI-Br** in ACN). These results further support the assumption that the transient species observed for **NI-PXZ** has significant CT character. Note that the absorption of the CS state of **NI-PXZ** is slightly different from the results obtained with spectroelectrochemistry study because of the interaction between the radical anion and cation in this compact dyad.[32]

The ns-TA spectra of **NI-DPA** were also studied (Supporting Information, Figure S41–43 in the Supporting Information). We observed a sharp ESA band centered at 360 nm, a GSB band centered at 450 nm and a second positive band above 460 nm. The triplet state lifetime was determined 95.1 μs in HEX (Figure S41 in the Supporting Information) and resulted *independent* on the solvent polarity (Figure S41–43 in the Supporting Information). This is drastically different from that of **NI-PXZ**.

In order to confirm the above proposed excited state dynamics of **NI-PXZ**, the *intermolecular* electron transfer between **NI** and **PXZ** was studied for a mixture of the two compounds in ACN (Figure S44 in the Supporting Information). Upon excitation of **NI** in the mixture, the spectrum of ^{3}NI* was initially observed, characterized by the ESA band centered at 470 nm. At longer delay times, the ESA band centered at 470 nm decreased, and at the same time, a sharp absorption band centered at 414 nm and a weaker, broader band centered at 527 nm developed. These two bands, attributed to the $NI^{-\bullet}$ and $PXZ^{+\bullet}$ absorption respectively, indicate that an inter-molecular charge separate state is formed. The evolution of the transient species was monitored at 410 nm (Figure S44c in the Supporting Information). An initial slow rise phase (2.21 μs) was observed, due to the generation of $NI^{-\bullet}$ via the inter-molecular CS (diffusion-controlled process). Successively a decay phase due to the inter-molecular CR, occurring in 24.3 μs, was determined.

Global fitting was applied to the ns-TA spectra of the mixture, retrieving the evolution-associated decay spectra (EADS) (Figure S44d in the Supporting Information). Only two spectra were identified for the ns-TA of the mixture: the first component represents the ^{3}NI* state absorption spectrum, with lifetime of 2.71 μs (much shorter than the compound **NI** alone under same experimental conditions, 58.9 μs). The second component is very close to the sum of the $NI^{-\bullet}$ and $PXZ^{+\bullet}$ abortions (see spectroelectrochemistry study, Figure 6), and is attributed to the inter-molecular CS state. The lifetime of the CS state was determined as 34.5 μs by the global fitting. However, it should be pointed out that the above transient *optical* absorption spectra cannot directly distinguish the spin multiplicity of the CS states. A powerful experimental method for distinguishing ^{1}CS and ^{3}CS state is the time-resolved electron paramagnetic resonance spectroscopy.

Time-resolved electron paramagnetic resonance (TREPR) spectroscopy

TREPR spectroscopy is a useful method to study the zero-field splitting of the triplet state (ZFS, characterized by *D* and *E* parameters), the ISC mechanism, the electron spin polarization (ESP) of the triplet state, and the electronic configuration of the paramagnetic transient species.[12a,c,18a,b,38] Previously we used TREPR spectroscopy to study the ISC and the triplet state of **NI-PTZ** compact dyad, observing a delocalized triplet state and a ^{3}CT state.[16a] Our recent studies on compact electron donor-acceptor dyads show that the electron spin chemistry is probably more complicated than previously thought.[12c,14c,26c] Therefore, we also used TREPR spectroscopy to study the current compounds.

First, the TREPR spectra of the reference compounds **NI** and **NI-Br** were studied (Figure 11). The spectra are typical for the triplet state of randomly oriented molecules in a magnetic field. The ESP phase pattern of the triplet state spectrum of **NI** is (*e*, *e*, *e*, *a*, *a*, *a*), which is typical for the triplet state of an organic chromophore populated via the ordinary spin orbit coupling (SOC)-ISC mechanism. The same pattern was observed for **NI-Br**, although the transitions at some canonical orientation are less pronounced (Figure 11b). Simulation of the spectrum of **NI** gives ZFS $|D|$ and $|E|$ parameters 2475 MHz and 135 MHz, respectively (Table 5). Slightly different $|D|$ and $|E|$ parameters were observed for **NI-Br**: 2527 MHz and 128 MHz, respectively. Interestingly, the population rates of the three sublevels of the T_1 state of **NI** and **NI-Br** are different (Table 5). We observed anisotropic relaxation of the signal at the canonical orientations (Figure S45 in the Supporting Information), which can be attributed to the different relaxation of the sublevels of the triplet state.[39]

The TREPR spectra of **NI-DPA** were also studied (Figure 11c, d). Interestingly, two triplet states are required to attain a satisfactory simulation of the spectrum, i.e. a NI-localized SOC triplet with characteristic $|D|$, $|E|$ parameters of NI moiety, and

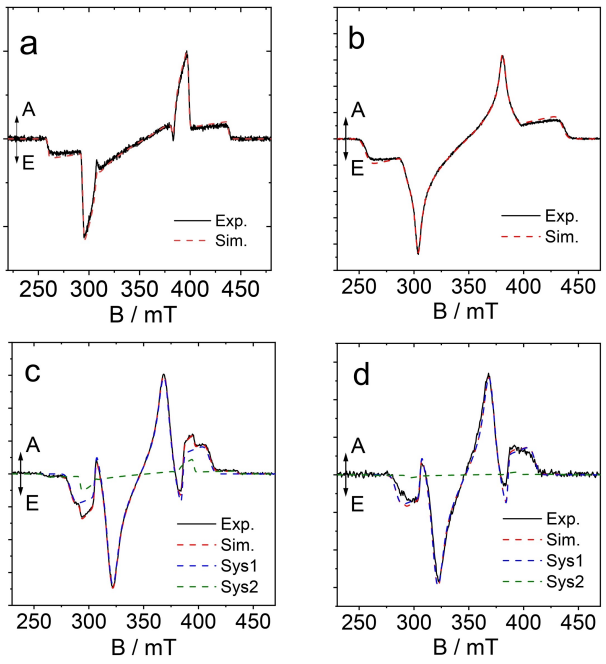

Figure 11. TREPR spectra of (a) **NI**, (b) **NI-Br** at time delay corresponding to the maximum of kinetics. TREPR spectra of **NI-DPA** at (c) short delays (the maximum of kinetics) and (d) long delays and corresponding simulations. 'Sys2' refers to NI-localized triplet, 'Sys1' to, supposedly, delocalized triplet state. 'Sim' is the sum of two contributions, and 'Exp' is experimental spectrum. The laser excitation wavelength is 355 nm; solvent is 2-MeTHF:TOL (1:3, v/v); T = 80 K.

another triplet with different $|D|$ and $|E|$ parameters. For the component with larger $|D|$ parameter (2475 MHz), the ESP phase pattern is (*e*, *e*, *a*, *e*, *a*, *a*), whereas for the component with smaller $|D|$ parameter (1773 MHz), the ESP phase pattern is (*e*, *a*, *e*, *a*, *e*, *a*). We assign these two triplet states to a NI confined triplet state and a delocalized triplet state, respectively, and the later has a smaller $|D|$ parameter.[16a,18a] This conclusion is supported by the electron spin density surface analysis (see later section). No fully charge separated state is expected, due to the non-vanishing $|E|$ parameter (151 MHz).[18a]

The spectrum of **NI-PXZ** is the most complicated in the series of the compounds. In toluene, it evolves from the very short delays (300 ns) after the laser flash, till the very long time

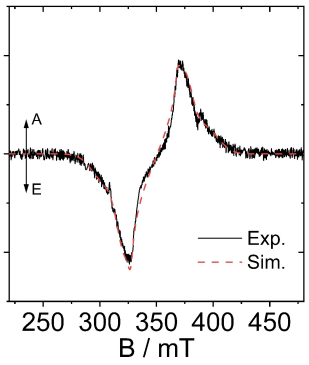

Figure 12. TREPR spectra of **NI-PXZ** at the maximum of the kinetics and corresponding simulation. The laser excitation wavelength is 355 nm; solvent is 2-MeTHF:TOL (1:3, v/v); T = 80 K.

delays, such as 57.8 μs (Figure S45 in the Supporting Information).

The simulation of the **NI-PXZ** spectrum in 2MeTHF:TOL (1:3, v/v) is shown in Figure 12. The shape of the spectrum and its characteristic splitting are most plausibly explained in the model of two triplet states undergoing a fast spin exchange between each other, the manifestation being generally similar to some previous reports.[40] In case of **NI-PXZ**, the DFT calculations together with the experimental triplet energy values, the TADF luminescence and nanosecond transient absorption spectra, suggest that exchange occurs between ^{3}LE and ^{3}CT states (see below). The exact calculation of the TREPR spectrum of two triplets undergoing spin exchange of arbitrary rate is challenging; however, well-known simplifications are possible in the limiting cases of slow or fast exchange. If exchange is fast, for each orientation of molecule relative to magnetic field the corresponding EPR lines at distinct positions coalesce into a single line at their center of gravity, and the apparent ZFS values correspond to the mean of those for individual tensors ($\mathbf{D_{eff}} = (\mathbf{D_1} + \mathbf{D_2})/2$).

Under assumption of a fast exchange, the TREPR spectrum of **NI-PXZ** can be well simulated, and the obtained effective ZFS parameters are $|D_{eff}| = 1484$ MHz and $|E_{eff}| = 109$ MHz (Table 5). The ZFS parameters *D* and *E* of pure **NI** are 2475 and 135 MHz, respectively. Thus, assuming $\mathbf{D_{eff}} = [D_{eff}, E_{eff}] = [1484, 109]$ MHz and $\mathbf{D_1} = \mathbf{D_{NI}} = [D_1, E_1] = [2475, 135]$ MHz, we can evaluate $\mathbf{D_2} = 2\mathbf{D_{eff}} - \mathbf{D_1}$ of the partner of **NI** in spin exchange, yielding $\mathbf{D_2} = [D_2,$

Table 5. The following parameters were used in simulations. ZFS parameters ($|D|$ and $|E|$) and relative population rates *Px,y,z* of the zero-field spin states of the NI derivatives.[a]

	$\lvert D\rvert$; $\lvert E\rvert$ [MHz]	$P_x:P_y:P_z$	ΔP[d]	Assignment
NI	[2475; 135]	0.19:1.00:0.00	0.81	^{3}NI
NI-Br	[2527; 128]	1.00:0.57:0.00	0.75	^{3}NI
NI-DPA[b]	[1773; 151], Sys1	1.00:0.09:0.00	10.1	delocalized triplet state
	[2475; 135], Sys2	0.19:1.00:0.00	0.81	^{3}NI
NI-PXZ[c]	[1484; 109]	0.75:1.00:0.00	0.25	^{3}NI-^{3}CT state exchange

[a] Obtained from simulations of the triplet-state TREPR spectra of the indicated molecules in toluene at 80 K. [b] Two different triplet states were used for the simulation; see Figure 11 in the main text for details. [c] The parameters of the simulation are an effective description of the spin exchange (see the main text). [d] $\Delta P = |P_x - P_y| / |P_y - P_z|$.

E_2] = [493, 83] MHz (here we also assume that the main axes are collinear for the two D-tensors). The value of D_2 is roughly 5 times smaller compared to D_1 of **NI**, which implies in a point dipole approximation that spin density is ~1.7 times more delocalized. This is a crude approximation, but it certainly points out that **NI**-localized triplet state exchanges with a more delocalized state, which can well be a ^{3}CT state (see below). Note that the effective broadening necessary for simulation of **NI-PXZ** spectrum also supports the exchange hypothesis. The values of broadening along X, Y and Z axes of molecular frame are not equal, being [70; 336; 693] MHz, respectively. Under above assumption of collinear main axes, individual X-components of the two exchanging states are closest to each other, whereas Z-components are most distant from each other. Therefore, exchange narrowing should be most effective for coalesced X-component and least effective for coalesced Z-component, exactly as is observed in simulation. Note that similar analysis of populations in spin-polarized exchanging triplets is more challenging, and the population rates given in Table 5 for **NI-PXZ** refer to the spin-exchanged spectrum. It should also be noted that this apparent ESP pattern is not typical for those formed via RP-ISC, i.e. (*a*, *e*, *e*, *a*, *a*, *e*) or (*e*, *a*, *a*, *e*, *e*, *a*), which is different from the previous reports on carbazole isophthalonitrile/triazole derived TADF molecules, where no exchange between two triplet states occurred.[18a]

An alternative explanation to a spin exchange between two triplet states could be strongly anisotropic relaxation of the spectrum, which sometimes leads to unusual line shapes and polarization patterns.[41–43] However, as is shown above, energetic arguments in case of **NI-PXZ** are in favor of the fast exchange hypothesis.

DFT computations

DFT theoretical calculations can help explain the above experimental phenomena. The optimized ground state geometry of **NI-PXZ** at DFT-CAM-B3LYP/6-31G (d) level with Gaussian 09. (Figure 13) shows that the dihedral angle between the PXZ and NI moieties is 96.2°, close to that previously reported for the **NI-PTZ** analogue (84.9°).[16a] However, while PTZ at ground state presents a puckered conformation (the dihedral angle between the two rings is ca. 135°),[25b] the geometry of PXZ is planar. We also optimized the excited state geometry, finding that in the singlet excited state the two moieties are close to be in orthogonal configuration, which is beneficial for SOCT-ISC.

The triplet state spin density surface of **NI-PXZ** was analyzed (Figure 14). For **NI-PXZ** in vacuum (approximated as in non-polar solvent), the triplet state density is mainly confined on the NI moiety, but the delocalization to the PXZ moiety is non-negligible. This is in agreement with the ns-TA spectral study, showing that the triplet state is neither a pure ^{3}NI state, nor a pure ^{3}CT state (Figure 10). The dihedral angle between the NI and PXZ moieties is 64.4° at the optimized T_1 state geometry. This more planar configuration at the T_1 state is opposite to some typical TADF molecules.[44] But it is in agreement with the small ZFS $|D|$ magnitude observed for the triplet state of **NI-PXZ** (Figure 12 and Table 5). In the polar solvent ACN, the spin density surface of the T_1 state is fully delocalized on both NI and PXZ moieties, thus we suppose it is a full CS state, in agreement with the ns-TA spectral studies (Figure 10). The dihedral angle between the NI and PXZ moieties is 90.2°. The spin density of the radical cation and radical anion of **NI-PXZ** were also studied by computation, and result confined on the PXZ and the NI moiety, respectively. This is in agreement with the spectroelectrochemical studies, showing that the radical cation and anion are highly confined.

The computed T_1 state (LE) energy is 2.23 eV, which is close the previously reported phosphorescence of the bromo-NI analogue (2.25 eV).[19b] It is also in agreement with our observation of the phosphorescence of **NI-Br** (Figure 4 and Figure S30 in the Supporting Information).

The photophysics of **NI-PXZ** is summarized in Scheme 2. In non-polar solvents such as HEX, both the ^{1}CS and ^{3}CS states share similar energy with the ^{3}NI state (2.23 eV), and TADF is observed. The ns-TA spectra confirm the co-existence of the ^{3}CS and the ^{3}NI states. This is also supported by the TREPR spectra, which indicates ^{3}LE and ^{3}CT states are in strong spin exchange interaction. In polar solvents, the CS state energy significantly decreases, the mixing with the ^{3}LE becomes negligible, thus TADF vanished. Based on fs-TA and the ns-TA data, we propose that the ^{3}CS state is populated, perhaps due to the weakly allowed ^{1}CS→^{3}LE and a very fast ^{3}LE→^{3}CS transition, while the up-hill reverse ISC, ^{3}CS→^{1}CS, is not-efficient so that no TADF is observed (at this time, the ^{3}LE and CS energy levels are not close). In the case of **NI-DPA**, because of the strong coupling between the NI and DPA moieties, the CS energy level is increased and the equilibrium process of ^{1}CS, ^{3}LE and ^{3}CS is

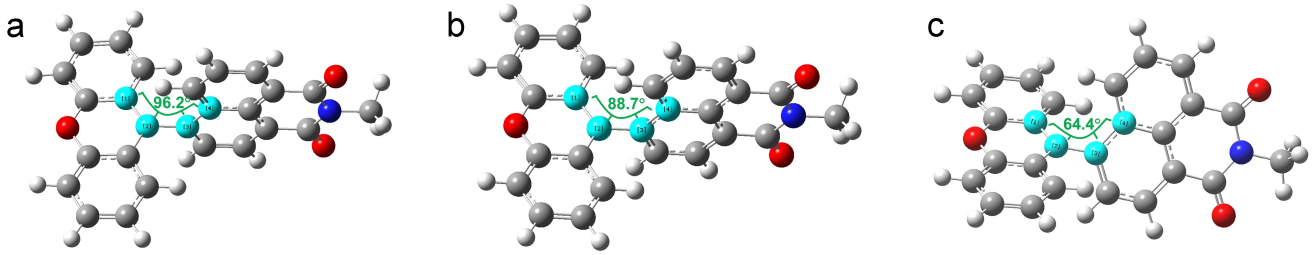

Figure 13. Dihedral angles of selected atoms of **NI-PXZ** at the optimized (a) ground state geometry (S_0), (b) singlet excited state (S_1) and (c) triplet excited state geometries (T_1). No solvent was considered in the calculation (vacuum). Calculated at DFT-CAM-B3LYP/6-31G (d) level with Gaussian 09.

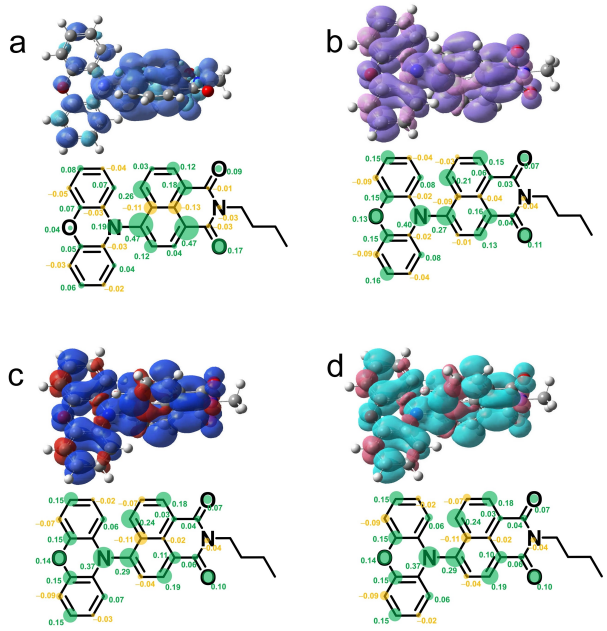

Figure 14. Spin density surfaces of triplet state of **NI-PXZ** in (a) vacuum, (b) CHX, (c) THF and (d) ACN. Calculated at the CAM-B3LYP/6-31G(d) level with Gaussian 09 (isoval = 0.0010).

destroyed, so TADF and long-lived CS states are not observed. **NI-PXZ** represents an solid evidence that an energetically closely-lying ^{3}LE state is essential for the TADF.[16a,18b]

Thermal properties and electroluminescent characteristics

The thermal properties of the compounds were evaluated using thermogravimetric analysis (TGA) and differential scanning calorimetry (DSC) (Figure S51 in the Supporting Information). We found that **NI-PXZ** has excellent thermal and morphological stability. The decomposition temperatures (T_d, corresponding to 5% weight loss) is ca. 285 °C, the glass transition temperatures (T_g, according to the second heating scan) were measured to be 73 °C, and the melting point (T_m) is ca. 225 °C. Therefore, the **NI-PXZ** has certain potential for application in the field of OLEDs.

To demonstrate that it is potentially useful in the lighting field, we fabricated a red TADF OLED based on **NI-PXZ** (the specific structure of the electroluminescent (EL) device is given in Supporting Information). The EL spectra characteristics and the plot of external quantum efficiency (EQE)-luminance and luminance-voltage-current density of the TADF OLEDs are depicted in Figure S52, and the corresponding device data are summarized in Table S5. The maximum values of external quantum efficiency (η_{ext}) of the devices is 1.28%, the EL spectra of the devices indicate that **NI-PXZ** is a red emitters with peak wavelengths of ca. 626 nm, and CIE coordinate of (0.609, 0.388). These results show that **NI-PXZ** can be used as a potential electroluminescent material with red TADF emission. During the preparation of this manuscript, application of similar compounds in OLED has been reported,[24a,45] however, the photophysical processes were not studied in detail. Based on the photophysical process, we can further gain insight into the luminescence mechanism and improve the performance of this TADF material.

Conclusion

In conclusion, we prepared a compact, orthogonal electron donor-acceptor dyad, with naphthalimide (NI) as electron acceptor and phenoxazine (PXZ) as electron donor. The two units are connected by a single C–N bond at the 4-position of the NI, and the *N* position of PXZ moiety, respectively, and they assume an orthogonal geometry, beneficial for the spin-orbit charge transfer intersystem crossing (SOCT-ISC). The dyad shows a weak charge transfer (CT) absorption band centered at 496 nm in the UV/Vis absorption spectrum, indicating non-negligible electronic coupling between the donor and acceptor at the ground state. Thermally activated delayed fluorescence (TADF) was observed in *n*-hexane where the luminescence decays with biexponential kinetics and components of 16.4 ns (99.2%)/17.0 μs (0.80%). No TADF was observed in polar solvents. Femtosecond transient absorption spectra show that

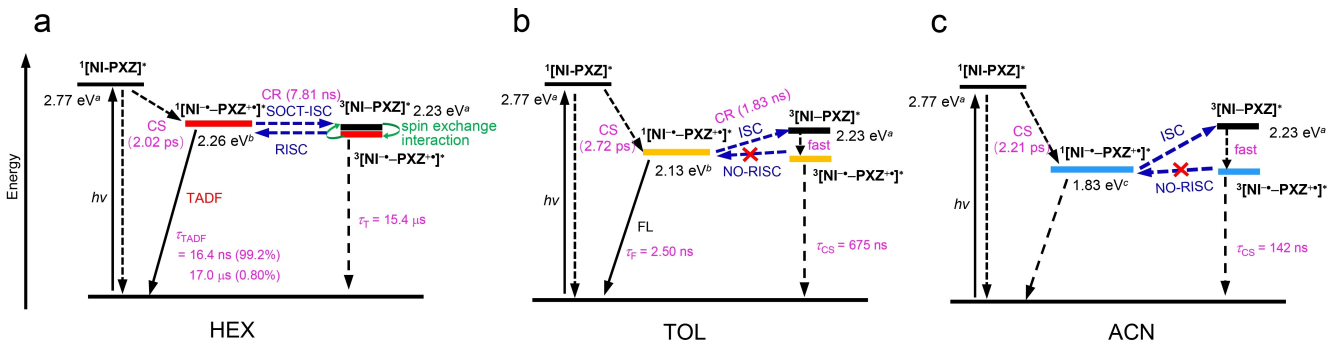

Scheme 2. Simplified Jablonski diagram illustrating the photophysical processes involved in **NI-PTZ** in *n*-hexane. (a) The ^{1}LE and triplet state energy is computed by TDDFT method, which were performed at the CAM-B3LYP/6-31G(d) level by using Gaussian09. (b) The ^{1}CT energy levels in HEX and TOL are approximated with the crossing point of CT absorption spectrum and CT emission spectrum. (c) The ^{1}CT energy levels in ACN are obtained from electrochemical data in Table 4.

the CS process is fast (ca. 2.02 ~ 2.72 ps, solvent polarity dependent), and the majority of the ^{1}CS state is short lived in polar solvents, for example it undergoes charge recombination (CR) in 10.3 ps in acetonitrile. The small residual ^{1}CS population undergoes ISC to produce ^{3}CS (probably mediated by the formation of ^{3}LE state) on a longer timescale (undetermined because of the very weak signal), and the CR from this triplet state takes 142 ns. Nanosecond transient absorption spectra show that the long-lived transient species with 15.4 μs lifetime, has mixed features of ^{3}LE and ^{3}CS states. This is supported by the spectroelectrochemical study of the radical anion and cation of the dyad, and the much longer triplet state lifetimes of the reference compounds (for NI and bromo-NI, triplet state lifetimes are 67.2 μs and 122 μs respectively). In polar solvents (THF and ACN), only the ^{3}CS state was observed on the long timescale, with lifetimes of 226 ns and 142 ns, respectively, indicating that ^{3}CS state has lower energy than the ^{3}NI state. Time-resolved electron paramagnetic resonance (TREPR) spectra show that the transient species of the dyad in frozen solution include two triplet states with ^{3}LE and ^{3}CS feature, respectively, and the two states are in strong spin exchange, with effective zero field splitting (ZFS) $|D|$ parameters of 1484 MHz and 109 MHz, respectively, which are much smaller than the native ^{3}NI states (2475 and 135 MHz, respectively), this is rare but solid evidence that an closely-lying and intermediate ^{3}LE state is essential for occurrence of TADF. The study of the TADF property of **NI-PXZ** shows that the ^{3}LE state is essential for the rISC in TADF, and a long-lived ^{3}CS state may be formed in a compact electron donor-acceptor dyad, for which the electron exchange (J) of the CS state is sufficient for formation of ^{3}CS state, instead of spin correlated radical pair.

Acknowledgements

J.Z., S.J. and Y.H. thank the National Science Foundation of China (U2001222), and the State Key Laboratory of Fine Chemicals for financial support. M.F. and I.K. thank the Ministry of Science and Higher Education of the Russian Federation (Grant No. 075-15-2020-779).

Conflict of Interest

The authors declare no conflict of interest.

Data Availability Statement

The data that support the findings of this study are available from the corresponding author upon reasonable request.

Keywords: charge transfer · intersystem crossing · naphthalimide · thermally activated delayed fluorescence · triplet state

[1] a) C. K. Prier, D. A. Rankic, D. W. C. MacMillan, *Chem. Rev.* **2013**, *113*, 5322–5363; b) A. Kamkaew, S. H. Lim, H. B. Lee, L. V. Kiew, L. Y. Chung, K. Burgess, *Chem. Soc. Rev.* **2013**, *42*, 77–88; c) X. Li, S. Kolemen, J. Yoon, E. U. Akkaya, *Adv. Funct. Mater.* **2017**, *27*, 1604053.

[2] a) Y. Cakmak, S. Kolemen, S. Duman, Y. Dede, Y. Dolen, B. Kilic, Z. Kostereli, L. T. Yildirim, A. L. Dogan, D. Guc, E. U. Akkaya, *Angew. Chem. Int. Ed.* **2011**, *50*, 11937–11941; *Angew. Chem.* **2011**, *123*, 12143–12147; b) T. Xiong, M. Li, Y. Chen, J. Du, J. Fan, X. Peng, *Chem. Sci.* **2021**, *12*, 2515–2520.

[3] a) X.-D. Wang, O. S. Wolfbeis, *Chem. Soc. Rev.* **2014**, *43*, 3666–3761; b) Y. Feng, J. Cheng, L. Zhou, X. Zhou, H. Xiang, *Analyst* **2012**, *137*, 4885–4901; c) S. Ji, W. Wu, W. Wu, P. Song, K. Han, Z. Wang, S. Liu, H. Guo, J. Zhao, *J. Mater. Chem.* **2010**, *20*, 1953–1963.

[4] a) D. P. Hari, B. König, *Chem. Commun.* **2014**, *50*, 6688–6699; b) S. Fukuzumi, K. Ohkubo, *Chem. Sci.* **2013**, *4*, 561–574; c) L. Shi, W. Xia, *Chem. Soc. Rev.* **2012**, *41*, 7687–7697; d) D. Ravelli, M. Fagnoni, A. Albini, *Chem. Soc. Rev.* **2013**, *42*, 97–113.

[5] a) T. N. Singh-Rachford, F. N. Castellano, *Coord. Chem. Rev.* **2010**, *254*, 2560–2573; b) J. Zhao, S. Ji, H. Guo, *RSC Adv.* **2011**, *1*, 937–950; c) J. Zhou, Q. Liu, W. Feng, Y. Sun, F. Li, *Chem. Rev.* **2015**, *115*, 395–465; d) N. Yanai, N. Kimizuka, *Acc. Chem. Res.* **2017**, *50*, 2487–2495; e) X. Guo, Y. Liu, Q. Chen, D. Zhao, Y. Ma, *Adv. Opt. Mater.* **2018**, *6*, 1700981; f) M. K. Manna, S. Shokri, G. P. Wiederrecht, D. J. Gosztola, A. J.-L. Ayitou, *Chem. Commun.* **2018**, *54*, 5809–5818.

[6] a) J. Zhao, W. Wu, J. Sun, S. Guo, *Chem. Soc. Rev.* **2013**, *42*, 5323–5351; b) J. Zhao, K. Xu, W. Yang, Z. Wang, F. Zhong, *Chem. Soc. Rev.* **2015**, *44*, 8904–8939.

[7] N. J. Turro, V. Ramamurthy, J. C. Scaiano, *Principles of Molecular Photochemistry: An Introduction*, University Science Books, Sausalito, CA, **2009**.

[8] a) M. Bröring, R. Krüger, S. Link, C. Kleeberg, S. Köhler, X. Xie, B. Ventura, L. Flamigni, *Chem. Eur. J.* **2008**, *14*, 2976–2983; b) B. Ventura, G. Marconi, M. Bröring, R. Krüger, L. Flamigni, *New J. Chem.* **2009**, *33*, 428–438.

[9] a) W. Wu, J. Zhao, J. Sun, S. Guo, *J. Org. Chem.* **2012**, *77*, 5305–5312; b) L. Huang, X. Yu, W. Wu, J. Zhao, *Org. Lett.* **2012**, *14*, 2594–2597; c) W.-J. Shi, M. E. El-Khouly, K. Ohkubo, S. Fukuzumi, D. K. P. Ng, *Chem. Eur. J.* **2013**, *19*, 11332–11341; d) Q. Zhou, M. Zhou, Y. Wei, X. Zhou, S. Liu, S. Zhang, B. Zhang, *Phys. Chem. Chem. Phys.* **2017**, *19*, 1516–1525.

[10] a) Z. Wang, J. Zhao, A. Barbon, A. Toffoletti, Y. Liu, Y. An, L. Xu, A. Karatay, H. G. Yaglioglu, E. A. Yildiz, M. Hayvali, *J. Am. Chem. Soc.* **2017**, *139*, 7831–7842; b) Z. Wang, Y. Gao, M. Hussain, S. Kundu, V. Rane, M. Hayvali, E. A. Yildiz, J. Zhao, H. G. Yaglioglu, R. Das, L. Luo, J. Li, *Chem. Eur. J.* **2018**, *24*, 18663–18675; c) X. Zhang, A. A. Sukhanov, E. A. Yildiz, Y. E. Kandrashkin, J. Zhao, H. G. Yaglioglu, V. K. Voronkova, *ChemPhysChem* **2021**, *22*, 55–68.

[11] a) Y. Wu, Y. Zhen, Y. Ma, R. Zheng, Z. Wang, H. Fu, *J. Phys. Chem. Lett.* **2010**, *1*, 2499–2502; b) K. Nagarajan, A. R. Mallia, K. Muraleedharan, M. Hariharan, *Chem. Sci.* **2017**, *8*, 1776–1782; c) Z. Wang, L. Huang, Y. Yan, A. M. El-Zohry, A. Toffoletti, J. Zhao, A. Barbon, B. Dick, O. F. Mohammed, G. Han, *Angew. Chem. Int. Ed.* **2020**, *59*, 16114–16121; *Angew. Chem.* **2020**, *132*, 16248–16255; d) Y. Dong, M. Taddei, S. Doria, L. Bussotti, J. Zhao, G. Mazzone, M. Di Donato, *J. Phys. Chem. B* **2021**, *125*, 4779–4793; e) Y. Dong, P. Kumar, P. Maity, I. Kurganskii, S. Li, A. Elmali, J. Zhao, D. Escudero, H. Wu, A. Karatay, O. F. Mohammed, M. Fedin, *Phys. Chem. Chem. Phys.* **2021**, *23*, 8641–8652.

[12] a) J. W. Verhoeven, *J. Photochem. Photobiol. C* **2006**, *7*, 40–60; b) S. Fukuzumi, *Pure Appl. Chem.* **2007**, *79*, 981–991; c) Y. Hou, X. Zhang, K. Chen, D. Liu, Z. Wang, Q. Liu, J. Zhao, A. Barbon, *J. Mater. Chem. C* **2019**, *7*, 12048–12074.

[13] a) J. W. Verhoeven, H. J. van Ramesdonk, M. M. Groeneveld, A. C. Benniston, A. Harriman, *ChemPhysChem* **2005**, *6*, 2251–2260; b) N. Zarrabi, B. J. Bayard, S. Seetharaman, N. Holzer, P. Karr, S. Ciuti, A. Barbon, M. Di Valentin, A. van der Est, F. D'Souza, P. K. Poddutoori, *Phys. Chem. Chem. Phys.* **2021**, *23*, 960–970.

[14] a) H. van Willigen, G. Jones, M. S. Farahat, *J. Phys. Chem.* **1996**, *100*, 3312–3316; b) Z. E. X. Dance, S. M. Mickley, T. M. Wilson, A. B. Ricks, A. M. Scott, M. A. Ratner, M. R. Wasielewski, *J. Phys. Chem. A* **2008**, *112*, 4194–4201; c) Z. Wang, A. A. Sukhanov, A. Toffoletti, F. Sadiq, J. Zhao, A. Barbon, V. K. Voronkova, B. Dick, *J. Phys. Chem. C* **2019**, *123*, 265–274; d) W. Hu, M. Liu, X.-F. Zhang, Y. Wang, Y. Wang, H. Lan, H. Zhao, *J. Phys. Chem. C* **2019**, *123*, 15944–15955; e) M. A. Filatov, S. Karuthedath, P. M. Polestshuk, H. Savoie, K. J. Flanagan, C. Sy, E. Sitte, M. Telitchko, F. Laquai, R. W. Boyle, M. O. Senge, *J. Am. Chem. Soc.* **2017**, *139*, 6282–6285; f) D. J. Gibbons, A. Farawar, P. Mazzella, S. Leroy-Lhez, R. M. Williams, *Photochem. Photobiol. Sci.* **2020**, *19*, 136–158; g) M. A. Filatov,

Org. Biomol. Chem. **2020**, *18*, 10–27; h) E. Bassan, A. Gualandi, P. G. Cozzi, P. Ceroni, *Chem. Sci.* **2021**, *12*, 6607–6628.
[15] Y. Hou, T. Biskup, S. Rein, Z. Wang, L. Bussotti, N. Russo, P. Foggi, J. Zhao, M. Di Donato, G. Mazzone, S. Weber, *J. Phys. Chem. C* **2018**, *122*, 27850–27865.
[16] a) G. Tang, A. A. Sukhanov, J. Zhao, W. Yang, Z. Wang, Q. Liu, V. K. Voronkova, M. Di Donato, D. Escudero, D. Jacquemin, *J. Phys. Chem. C* **2019**, *123*, 30171–30186; b) F. Ni, N. Li, L. Zhan, C. Yang, *Adv. Opt. Mater.* **2020**, *8*, 1902187; c) Y. Im, S. Y. Byun, J. H. Kim, D. R. Lee, C. S. Oh, K. S. Yook, J. Y. Lee, *Adv. Funct. Mater.* **2017**, *27*, 1603007; d) M. Y. Wong, E. Zysman-Colman, *Adv. Mater.* **2017**, *29*, 1605444; e) X. Cao, D. Zhang, S. Zhang, Y. Tao, W. Huang, *J. Mater. Chem. C* **2017**, *5*, 7699–7714.
[17] H. Uoyama, K. Goushi, K. Shizu, H. Nomura, C. Adachi, *Nature* **2012**, *492*, 234–238.
[18] a) T. Ogiwara, Y. Wakikawa, T. Ikoma, *J. Phys. Chem. A* **2015**, *119*, 3415–3418; b) B. H. Drummond, N. Aizawa, Y. Zhang, W. K. Myers, Y. Xiong, M. W. Cooper, S. Barlow, Q. Gu, L. R. Weiss, A. J. Gillett, D. Credgington, Y.-J. Pu, S. R. Marder, E. W. Evans, *Nat. Commun.* **2021**, *12*, 4532; c) H. Noda, X.-K. Chen, H. Nakanotani, T. Hosokai, M. Miyajima, N. Notsuka, Y. Kashima, J.-L. Brédas, C. Adachi, *Nat. Mater.* **2019**, *18*, 1084–1090; d) F. B. Dias, J. Santos, D. R. Graves, P. Data, R. S. Nobuyasu, M. A. Fox, A. S. Batsanov, T. Palmeira, M. N. Berberan-Santos, M. R. Bryce, A. P. Monkman, *Adv. Sci.* **2016**, *3*, 1600080.
[19] a) G. P. Wiederrecht, W. A. Svec, M. R. Wasielewski, T. Galili, H. Levanon, *J. Am. Chem. Soc.* **1999**, *121*, 7726–7727; b) B. Ventura, A. Bertocco, D. Braga, L. Catalano, S. d'Agostino, F. Grepioni, P. Taddei, *J. Phys. Chem. C* **2014**, *118*, 18646–18658; c) F. Doria, I. Manet, V. Grande, S. Monti, M. Freccero, *J. Org. Chem.* **2013**, *78*, 8065–8073.
[20] A. Samanta, B. Ramachandram, G. Saroja, *J. Photochem. Photobiol. A* **1996**, *101*, 29–32.
[21] a) C. B. Kc, G. N. Lim, V. N. Nesterov, P. A. Karr, F. D'Souza, *Chem. Eur. J.* **2014**, *20*, 17100–17112; b) L. E. Shoer, S. W. Eaton, E. A. Margulies, M. R. Wasielewski, *J. Phys. Chem. B* **2015**, *119*, 7635–7643.
[22] a) M. Imran, A. A. Sukhanov, Z. Wang, A. Karatay, J. Zhao, Z. Mahmood, A. Elmali, V. K. Voronkova, M. Hayvali, Y. H. Xing, S. Weber, *J. Phys. Chem. C* **2019**, *123*, 7010–7024; b) X. Xiao, J. Pang, A. A. Sukhanov, Y. Hou, J. Zhao, M.-D. Li, V. K. Voronkova, *J. Chem. Phys.* **2020**, *153*, 184312.
[23] K. Chen, W. Yang, Z. Wang, A. Iagatti, L. Bussotti, P. Foggi, W. Ji, J. Zhao, M. Di Donato, *J. Phys. Chem. A* **2017**, *121*, 7550–7564.
[24] a) B. Wang, Y. Zheng, T. Wang, D. Ma, Q. Wang, *Org. Electron.* **2021**, *88*, 106012; b) S. Qi, S. Kim, V.-N. Nguyen, Y. Kim, G. Niu, G. Kim, S.-J. Kim, S. Park, J. Yoon, *ACS Appl. Mater. Interfaces* **2020**, *12*, 51293–51301; c) S. Jena, P. Dhanalakshmi, G. Bano, P. Thilagar, *J. Phys. Chem. B* **2020**, *124*, 5393–5406.
[25] a) A. Singhabhandhu, P. D. Robinson, J. H. Fang, W. E. Geiger, *Inorg. Chem.* **1975**, *14*, 318–323; b) Y. Hou, Q. Liu, J. Zhao, *Chem. Commun.* **2020**, *56*, 1721–1724.
[26] a) S. Sasaki, K. Hattori, K. Igawa, G.-I. Konishi, *J. Phys. Chem. A* **2015**, *119*, 4898–4906; b) K. Chen, M. Taddei, L. Bussotti, P. Foggi, J. Zhao, M. Di Donato, *ChemPhotoChem* **2020**, *4*, 487–501; c) Y. Dong, A. A. Sukhanov, J. Zhao, A. Elmali, X. Li, B. Dick, A. Karatay, V. K. Voronkova, *J. Phys. Chem. C* **2019**, *123*, 22793–22811; d) Z. Wang, J. Zhao, M. Di Donato, G. Mazzone, *Chem. Commun.* **2019**, *55*, 1510–1513.
[27] H. Tanaka, K. Shizu, H. Miyazaki, C. Adachi, *Chem. Commun.* **2012**, *48*, 11392–11394.
[28] X. Liu, Q. Qiao, W. Tian, W. Liu, J. Chen, M. J. Lang, Z. Xu, *J. Am. Chem. Soc.* **2016**, *138*, 6960–6963.
[29] T. Gerbich, H.-C. Schmitt, I. Fischer, R. Mitrić, J. Petersen, *J. Phys. Chem. A* **2016**, *120*, 2089–2095.
[30] a) D. I. Schuster, P. Cheng, P. D. Jarowski, D. M. Guldi, C. Luo, L. Echegoyen, S. Pyo, A. R. Holzwarth, S. E. Braslavsky, R. M. Williams, G. Klihm, *J. Am. Chem. Soc.* **2004**, *126*, 7257–7270; b) E. H. Yonemoto, G. B. Saupe, R. H. Schmehl, S. M. Hubig, R. L. Riley, B. L. Iverson, T. E. Mallouk, *J. Am. Chem. Soc.* **1994**, *116*, 4786–4795.
[31] D. Liu, A. M. El-Zohry, M. Taddei, C. Matt, L. Bussotti, Z. Wang, J. Zhao, O. F. Mohammed, M. Di Donato, S. Weber, *Angew. Chem. Int. Ed.* **2020**, *59*, 11591–11599; *Angew. Chem.* **2020**, *132*, 11688–11696.
[32] A. Karimata, H. Kawauchi, S. Suzuki, M. Kozaki, N. Ikeda, K. Keyaki, K. Nozaki, K. Akiyama, K. Okada, *Chem. Lett.* **2013**, *42*, 794–796.
[33] N. Pearce, E. S. Davies, R. Horvath, C. R. Pfeiffer, X.-Z. Sun, W. Lewis, J. McMaster, M. W. George, N. R. Champness, *Phys. Chem. Chem. Phys.* **2018**, *20*, 752–764.
[34] S. I. van Dijk, C. P. Groen, F. Hartl, A. M. Brouwer, J. W. Verhoeven, *J. Am. Chem. Soc.* **1996**, *118*, 8425–8432.
[35] T. Akasaka, A. Nakata, M. Rudolf, W.-W. Wang, M. Yamada, M. Suzuki, Y. Maeda, R. Aoyama, T. Tsuchiya, S. Nagase, D. M. Guldi, *ChemPlusChem* **2017**, *82*, 1067–1072.
[36] a) D. W. Cho, M. Fujitsuka, U. C. Yoon, T. Majima, *J. Photochem. Photobiol. A* **2007**, *190*, 101–109; b) D. W. Cho, M. Fujitsuka, A. Sugimoto, U. C. Yoon, D. W. Cho, T. Majima, *Phys. Chem. Chem. Phys.* **2014**, *16*, 5779–5784; c) D. W. Cho, M. Fujitsuka, A. Sugimoto, U. C. Yoon, P. S. Mariano, T. Majima, *J. Phys. Chem. B* **2006**, *110*, 11062–11068.
[37] S. Fukuzumi, *Org. Biomol. Chem.* **2003**, *1*, 609–620.
[38] S. Richert, C. E. Tait, C. R. Timmel, *J. Magn. Reson.* **2017**, *280*, 103–116.
[39] Z. Wang, A. Toffoletti, Y. Hou, J. Zhao, A. Barbon, B. Dick, *Chem. Sci.* **2021**, *12*, 2829–2840.
[40] a) Y. E. Kandrashkin, M. D. Valentin, A. V. d Est, *J. Chem. Phys.* **2020**, *153*, 094304; b) A. Blank, H. Levanon, *Concepts Magn. Reson. Part A* **2005**, *25 A*, 18–39.
[41] G. P. Wiederrecht, W. A. Svec, M. R. Wasielewski, T. Galili, H. Levanon, *J. Am. Chem. Soc.* **2000**, *122*, 9715–9722.
[42] a) M. T. Colvin, A. B. Ricks, A. M. Scott, A. L. Smeigh, R. Carmieli, T. Miura, M. R. Wasielewski, *J. Am. Chem. Soc.* **2011**, *133*, 1240–1243; b) M. T. Colvin, A. B. Ricks, A. M. Scott, D. T. Co, M. R. Wasielewski, *J. Phys. Chem. A* **2012**, *116*, 1923–1930.
[43] F. J. Adrian, L. Monchick, *J. Chem. Phys.* **1979**, *71*, 2600–2610.
[44] W. Zhang, H. Song, J. Kong, Z. Kuang, M. Li, Q. Guo, C.-F. Chen, A. Xia, *J. Phys. Chem. C* **2019**, *123*, 19322–19332.
[45] N. Masimukku, D. Gudeika, D. Volyniuk, O. Bezvikonnyi, J. Simokaitiene, V. Matulis, D. Lyakhov, V. Azovskyid, J. V. Gražulevicius, *Phys. Chem. Chem. Phys.* **2022**, *24*, 5070–5082.

Manuscript received: February 17, 2022
Accepted manuscript online: April 19, 2022
Version of record online: May 23, 2022